Atherosclerosis 251 (2016) 381–388

Contents lists available at ScienceDirect

Atherosclerosis

journal homepage: www.elsevier.com/locate/atherosclerosis

HDL mimetic CER-001 targets atherosclerotic plaques in patients

Kang He Zheng [a], Fleur M. van der Valk [a], Loek P. Smits [a], Mara Sandberg [a], Jean-Louis Dasseux [b], Rudi Baron [b], Ronald Barbaras [b], Constance Keyserling [b], Bram F. Coolen [c], Aart J. Nederveen [c], Hein J. Verberne [d], Thijs E. Nell [e], Danielle J. Vugts [e], Raphaël Duivenvoorden [a], Zahi A. Fayad [f], Willem J.M. Mulder [a, f], Guus A.M.S. van Dongen [e], Erik S.G. Stroes [a, *]

[a] Department of Vascular Medicine, Academic Medical Center, Amsterdam, The Netherlands
[b] Cerenis Therapeutics Holding, Toulouse, France
[c] Department of Radiology, Academic Medical Center, Amsterdam, The Netherlands
[d] Department of Nuclear Medicine, Academic Medical Center, Amsterdam, The Netherlands
[e] Department of Radiology and Nuclear Medicine, VU University Medical Center, Amsterdam, The Netherlands
[f] Translational and Molecular Imaging Institute, Icahn School of Medicine at Mount Sinai, New York, USA

ARTICLE INFO

Article history:
Received 24 March 2016
Received in revised form
9 May 2016
Accepted 25 May 2016
Available online 27 May 2016

Keywords:
Imaging
PET/CT
MRI
HDL mimetic
CER-001
Apolipoprotein A-I
Zirconium-89
Nanomedicine

ABSTRACT

Background and aims: Infusion of high-density lipoprotein (HDL) mimetics aimed at reducing atherosclerotic burden has led to equivocal results, which may relate in part to the inability of HDL mimetics to adequately reach atherosclerotic lesions in humans. This study evaluated delivery of recombinant human apolipoprotein A-I (apoA-I) containing HDL mimetic CER-001 in carotid plaques in patients.

Methods: CER-001 was radiolabeled with the long-lived positron emitter zirconium-89 (^{89}Zr) to enable positron emission tomography with computed tomography (PET/CT) imaging. Eight patients with atherosclerotic carotid artery disease (>50% stenosis) received a single infusion of unlabeled CER-001 (3 mg/kg), co-administered with 10 mg of ^{89}Zr-labeled CER-001 (18 MBq). Serial PET/CT imaging and contrast enhanced-magnetic resonance imaging (CE-MRI) were performed to evaluate targeted delivery of CER-001.

Results: One hour after infusion, mean plasma apoA-I levels increased by 9.9 mg/dL ($p = 0.026$), with a concomitant relative increase in the plasma cholesterol efflux capacity of 13.8% ($p < 0.001$). Using serial PET/CT imaging, we showed that arterial uptake of CER-001 expressed as target-to-background ratio (TBR_{max}) increased significantly 24 h after infusion, and remained increased up to 48 h (TBR_{max} t = 10 min: 0.98; t = 24 h: 1.14 ($p = 0.001$); t = 48 h: 1.12 ($p = 0.007$)). TBR_{max} was higher in plaque compared with non-plaque segments (1.18 *vs.* 1.05; $p < 0.001$). Plaque TBR_{max} correlated with local plaque contrast enhancement ($r = 0.56$; $p = 0.019$) as assessed by CE-MRI.

Conclusions: Infusion of HDL mimetic CER-001 increases plasma apoA-I concentration and plasma cholesterol efflux capacity. Our data support the concept that CER-001 targets plaque regions in patients, which correlates with plaque contrast enhancement. These clinical findings may also guide future nanomedicine development using HDL particles for drug delivery in atherosclerosis.

Clinical trial registration: Netherlands Trial Registry – NTR5178.
http://www.trialregister.nl/trialreg/admin/rctview.asp?TC=5178.

* Corresponding author. Academic Medical Center, Department of Vascular Medicine, Meibergdreef 9, 1105 AZ Amsterdam, The Netherlands.
E-mail addresses: k.h.zheng@amc.nl (K.H. Zheng), f.m.valkvander@amc.nl (F.M. van der Valk), l.p.smits@amc.nl (L.P. Smits), marasandberg@hotmail.com (M. Sandberg), dasseux@cerenis.com (J.-L. Dasseux), baron_rudi@yahoo.fr (R. Baron), barbaras@cerenis.com (R. Barbaras), keyserling@cerenis.com (C. Keyserling), b.f.coolen@amc.nl (B.F. Coolen), a.j.nederveen@amc.nl (A.J. Nederveen), h.j.verberne@amc.nl (H.J. Verberne), t.nell@vumc.nl (T.E. Nell), d.vugts@vumc.nl (D.J. Vugts), raphael.duivenvoorden@gmail.com (R. Duivenvoorden), zahi.fayad@mssm.edu (Z.A. Fayad), wjmmulder@gmail.com (W.J.M. Mulder), GAMS.vanDongen@vumc.nl (G.A.M.S. van Dongen), e.s.stroes@amc.nl (E.S.G. Stroes).

http://dx.doi.org/10.1016/j.atherosclerosis.2016.05.038

1. Introduction

Despite the strong inverse relationship between high-density lipoprotein (HDL) cholesterol concentration and cardiovascular disease (CVD) risk in epidemiological surveys [1], therapies aimed at pharmacologically raising HDL cholesterol levels consistently failed to reduce CVD [2–6]. It was subsequently suggested that the cholesterol load carried by the HDL particle may not be the best reflection of the atheroprotective effect of the apolipoproteinA-1/HDL (apoA-I) complex [7]. The best documented, protective effect of HDL relates to its role in mediating reverse cholesterol transport from peripheral tissues [8], including lipid-laden macrophages in plaques, to the liver [9]. This process is predominantly mediated via the cholesterol efflux channel ATP-binding cassette transporter A1 (ABCA1) for which lipid-poor apoA-I serves as the preferred cholesterol acceptor. The clinical relevance of this route is underscored by a recent study describing an independent predictive effect of ABCA1-mediated cholesterol efflux capacity for future CVD risk [10]. In support, preclinical animal models corroborated a beneficial effect of apoA-I gene therapy [11] and of infusion of apoA-I-containing HDL mimetics [12,13] by inducing regression of atherosclerotic plaques. Hence, increasing the number of apoA-I-containing HDL particles constitutes a potentially attractive target for CVD risk reduction [14].

In humans, early proof-of-concept studies reported lipid removal from femoral atherosclerotic plaques in CVD patients following a single infusion of reconstituted HDL-like particles [15]. However, randomized, placebo-controlled trials failed to substantiate these findings in coronary atherosclerosis. Infusion of the HDL mimetics ETC-216 (apoA-I Milano complex) [16], CSL-111 [17], and CER-001 [18], in patients following an acute coronary syndrome showed reduction of plaque atheroma volume measured by intravascular ultrasound versus baseline, but not compared with placebo. Conversely, CER-001 reduced plaque atheroma volume assessed by intravascular ultrasound in patients with plaque atheroma volume $\geq$30% at baseline [19]. Furthermore, CER-001 reduced carotid arterial wall area assessed by magnetic resonance imaging (MRI) in patients with familial hypoalphalipoproteinemia [20], as well as homozygous familial hypercholesterolemia [21]. The observed reductions coincided with CER-001-induced increase in plasma cholesterol efflux capacity [20]. The discrepant responses may have several explanations, such as insufficient dosing of apoA-I HDL mimetics, or the induction of dysfunctional HDL particles in patients with atherosclerotic risk factors [22,23]. Another important factor may relate to differences in the permeability of atherosclerotic plaques, precluding apoA-I HDL from accessing advanced plaques. Although localization of infused HDL particles in murine plaques has been reported by earlier studies [24,25], their entry in human atherosclerotic plaques has not been documented.

Here, we evaluated whether the intravenously infused apoA-I containing HDL mimetic CER-001 accessed plaques in patients with advanced carotid artery stenosis. We labeled the apoA-I component of CER-001 with the radionuclide zirconium-89 (^{89}Zr; $t_{1/2}$ = 78.4 h) and performed serial quantification of the arterial wall using positron emission tomography with computed tomography (PET/CT) imaging. We also investigated whether local accessibility of ^{89}Zr-labeled CER-001 was related to plaque contrast enhancement assessed by contrast enhanced (CE)-MRI. Furthermore, the effect of ^{89}Zr-labeled CER-001 on cholesterol efflux capacity was measured *in vitro* in J774-macrophages, and *in vivo* in C57Bl6/J mice, as well as in the plasma of all patients.

2. Materials and methods

2.1. Study design

This single-center observational study was conducted in accordance with the Declaration of Helsinki and in compliance with current Good Clinical Practice guidelines. The protocol was approved by the local institutional review board, and all participants provided written informed consent. Each patient received a single infusion of CER-001 (3 mg/kg bodyweight) which was co-administered with ^{89}Zr-labeled CER-001 (10 mg−18 MBq), during a timeframe of 1 h. To non-invasively and serially trace the ^{89}Zr-labeled CER-001 particles, a PET/CT scan was performed 10 min, 24 h, and 48 h after infusion. Subsequently, all patients underwent a contrast enhanced-magnetic resonance imaging (CE-MRI) scan of the carotid arteries to assess plaque burden and contrast enhancement. The study flowchart is shown in Fig. 1.

2.2. CER-001

CER-001 is an engineered lipoprotein complex mimicking natural pre-beta HDL, consisting of recombinant human apoA-I and phospholipids. See Data Supplement for more details regarding CER-001.

2.3. Study participants

The study population comprised male and female patients >50 years of age with documented carotid artery stenosis ($\geq$50%) on ultrasonography. Exclusion criteria included contra-indications to PET/CT or CE-MRI, a recent cardiovascular event (<3 months prior to inclusion) and decreased renal function (creatinine clearance <50 mL/min).

2.4. Production and stability of ^{89}Zr-labeled CER-001

^{89}Zr-labeled CER-001 was synthesized according to Good Manufacturing Practice guidelines. The procedure for ^{89}Zr-radiolabeling has been described previously [26]. See Data Supplement for details regarding ^{89}Zr-labeling of CER-001.

2.5. Functionality of Zr-labeled CER-001

To assess whether the covalent coupling to the bifunctional chelator *p*-isothiocyanotobenzyl desferrioxamine (Df-Bz-NCS) and subsequent labeling with Zr affected the functionality of CER-001, the cholesterol mobilizing capacity of CER-001 labeled with natural non-radioactive Zr (^{nat}Zr) was compared with unmodified CER-001 *in vitro* and *in vivo*. J774-macrophages were seeded on 24-well plates (300,000 cells/well) and loaded with [^{3}H]-cholesterol oxidized low-density lipoprotein (LDL) (18.5 kBq/well) in Dulbecco's Modified Eagle's Medium/fetal calf serum (2.5%) for 24 h. After an overnight equilibration, [^{3}H]-cholesterol release was measured 6 h after incubation with CER-001 and ^{nat}Zr-labeled CER-001 in ascending doses. Assays were performed in triplicate. Cholesterol efflux was expressed as the percentage of radioactivity released from cells into the medium relative to the total radioactivity in cells and medium. To investigate *in vivo* cholesterol mobilization, C57Bl6/J mice received a 250 μg in 50 μL injection of CER-001 or ^{nat}Zr-labeled CER-001 after being fasted overnight. Blood was sampled from the caudal vein at different timepoints. The plasma unesterified cholesterol concentration was determined with the Biolabo Unesterified Cholesterol Kit (Biolabo, Maizy, France).

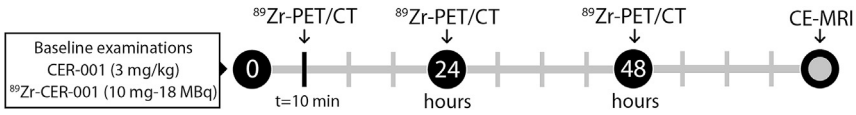

Fig. 1. Study flowchart. Scheme illustrating that 8 patients received an infusion of unlabeled CER-001 and ^{89}Zr-labeled CER-001, followed by 3 PET/CT scans (t = 10 min, 24 h, 48 h) and subsequently underwent CE-MRI scans. CE, contrast-enhanced.

2.6. PET/CT imaging

Patients in fasting state received a single infusion of CER-001 (3 mg/kg bodyweight) together with ^{89}Zr-labeled CER-001 (10 mg–18 MBq). PET/CT scans (Philips Gemini, Philips, Best, The Netherlands) of the carotid arteries were performed at 10 min, 24 h, and 48 h after infusion. An ultralow-dose non-contrast CT scan was performed for attenuation correction and co-registration. The radiation exposure for this study was estimated to be 18 mSv for each participant. Image analysis was performed as previously described [20,27] on a dedicated commercially available workstation (OsiriX 6.0, Pixmeo, Bernex, Switzerland). In brief, arterial ^{89}Zr–labeled CER-001 uptake was assessed by drawing regions of interests by delineating the arterial wall in a standardized segment of 5 sequential slices (25 mm) in the distal common carotid artery on the co-registered CT. The maximal standardized uptake value was calculated as the maximal pixel activity within each region of interest. For each artery, the maximal target-to-background-ratio (TBR_{max}) was calculated by correcting the mean maximal standardized uptake value of these regions for the mean background blood activity in the venous blood pool. To investigate whether ^{89}Zr-labeled CER-001 readily accessed plaques, MRI was used to identify plaque and non-plaque areas, and to co-localize these segments of the carotid arteries on PET/CT. Subsequently, regions of interest were drawn in these regions, and plaque and non-plaque TBR_{max} were calculated for each segment.

2.7. 3T MRI measurements

Carotid MRI was performed on a 3T MRI scanner (Philips Healthcare, Best, The Netherlands) using a dedicated bilateral 8-channel carotid coil (Shanghai Chenguang Medical Technologies, Shanghai, China). See Data Supplement for details regarding MRI sequence parameters. Arterial wall dimensions were analyzed in the standardized segment of the distal common carotid artery, the 25 mm directly proximal from the flow divider, corresponding to the area analyzed on PET/CT. The same was performed for all atherosclerotic plaques in the common and internal carotid artery, identified as segments with a maximal wall thickness of >2.0 mm that could be co-localized on PET/CT. For each plaque, a non-plaque segment of >10 mm length starting within 25 mm distance of the plaque in the same artery was identified. This non-plaque segment had the lowest mean wall thickness in that area and did not exceed a maximum wall thickness of 2.0 mm. Lumen and outer wall contours were drawn manually using dedicated software (Vessel-Mass, Leiden University Medical Center, Leiden, the Netherlands), after which the mean wall area, mean wall thickness, and maximal wall thickness were calculated for the common carotid arteries, individual plaques, and non-plaque segments.

To assess plaque contrast enhancement, three-dimensional delayed enhancement MRI was performed at baseline and 15 min after intravenous administration of Gadovist (0.1 mL/kg bodyweight, 1 mL/s). All atherosclerotic plaques with a maximal wall thickness greater than 2.0 mm in the common and internal carotid artery, and corresponding non-plaque segments were selected for delayed enhancement analysis. The degree of contrast enhancement was defined as the post-contrast/pre-contrast signal intensity ratio. For this analysis, we ensured equal signal scaling and negligible patient motion between pre- and post-contrast scans.

2.8. Plasma lipids, lipoprotein profiles and cholesterol efflux capacity

Total cholesterol, HDL-cholesterol, LDL-cholesterol, and triglycerides were measured by standard enzymatic methods (Diagnostic Systems, Holzheim, Germany) on a SELECTRA automated spectrophotometric analyzer (VitaLab, Dieren, The Netherlands). ApoA-I was measured with a turbidimetric assay (Diagnostic Systems, Holtzheim, Germany) using the SELECTRA analyzer. Cholesterol efflux capacity was quantified as described previously [28] using serum samples collected from patients before and after infusion of CER-001. See Data Supplement for details regarding the cholesterol efflux assay.

2.9. Safety

See Data Supplement for more details regarding safety monitoring.

2.10. Statistical analyses

Data are represented as means with standard deviations or medians with interquartile ranges. For evaluation of TBR_{max} change over time, repeated measures analysis of variance was performed. If significance was found, post-hoc tests with Bonferroni correction were performed to compare TBR_{max} at different timepoints. To assess differences in apoA-I levels and cholesterol efflux capacity after infusion, the paired Student *T*-test was performed. The Pearson correlation coefficient was used to assess the relationship between plaque PET/CT signal and contrast uptake. Statistical analyses were performed using the SPSS statistics software (Version 22.0, IBM, Armonk, NY, USA). A p-value of <0.05 was considered statistically significant.

3. Results

3.1. Stability of ^{89}Zr-labeled CER-001

Sulphate-polyacrylamide gel electrophoresis (SDS-PAGE) analysis of full blood samples showed >99% of the radioactivity in the HDL protein band after 24 and 48 h of incubation, with a slightly lower percentage for serum samples (Data Supplement Fig. 1B). On high-performance liquid chromatography (HPLC), ^{89}Zr-labeled CER-001 resulted in a single peak with retention time of 24.4 min (Data Supplement Fig. 1C). The same peak was observed upon incubation of ^{89}Zr-labeled CER-001 for 24 h in full blood. A second, small peak arose when ^{89}Zr-labeled CER-001 was incubated for 24 or 48 h in serum or for 48 h in full blood. Taking the SDS-PAGE data into account, the second peak seems more indicative for altered mobility of CER-001 on HPLC than for degradation as such. In addition, incubation with ^{89}Zr-labeled CER-001 in full blood for

24 h demonstrated that, after centrifugation, <3% of total gamma counts were in the cellular fraction.

3.2. Functionality of Zr-labeled CER-001

Prior to clinical evaluation of ^{89}Zr-labeled CER-001, the cholesterol mobilizing capacity of CER-001 was investigated as a quality test to assess any functional changes after Zr-labeling of CER-001. *In vitro* cholesterol efflux from J774 macrophages increased in a similar fashion in response to high concentrations of both CER-001 and ^{nat}Zr-labeled CER-001, reaching a plateau above 50 μg/mL for both formulations (Fig. 2A). In C57Bl6/J mice, injection of CER-001 and ^{nat}Zr-labeled CER-001 resulted in similar kinetics for the mobilization of unesterified cholesterol (Fig. 2B). These data indicate that covalent coupling of CER-001 with the bifunctional chelator Df-Bz-NCS and subsequent labeling with Zr does not affect its cholesterol-mobilizing capacity.

3.3. Baseline characteristics

To evaluate delivery of ^{89}Zr-labeled CER-001 to the carotid plaque, we included 8 patients, aged 66.8 ± 5.7 years, with carotid artery stenosis of at least 50% in one or both carotid arteries, as documented by ultrasound measurements. Clinical characteristics are listed in Table 1. All patients received standard of care medication for CVD. At baseline, HDL-cholesterol was 42.0 ± 12.6 mg/dL and mean apoA-I concentration was 157.9 ± 36.7 mg/dL.

3.4. ApoA-I and cholesterol efflux capacity

Following infusion of CER-001 and ^{89}Zr-labeled CER-001, apoA-I levels increased by 9.9 mg/dL after 1 h ($p = 0.026$; Fig. 3A), with a concomitant relative increase of 13.8% in plasma cholesterol efflux capacity ($p < 0.001$; Fig. 3B). After 24 h, apoA-I levels and cholesterol efflux capacity returned to pre-infusion values.

3.5. Multimodality imaging

To evaluate carotid artery uptake of ^{89}Zr-labeled CER-001, PET/CT imaging was performed 10 min, 24 h, and 48 h after infusion. All scans were suitable for image analysis of both carotid arteries, providing 48 carotid TBR_{max} values in total, representing both left and right carotid arteries at 3 timepoints in 8 patients. Directly after infusion (10 min), carotid TBR_{max} was 0.98 ± 0.12. Compared with the 10-min scans, carotid TBR_{max} increased to 1.14 ± 0.10 ($p = 0.001$) at 24 h and remained increased at 48 h post-infusion (1.12 ± 0.11, $p = 0.007$; Fig. 4A).

Table 1
Baseline clinical characteristics.

Clinical characteristic	Value (n = 8)
Carotid stenosis ≥50% on ultrasound, n (%)	
One carotid	3 (37.5%)
Both carotids	5 (62.5%)
Age, years (mean ± SD)	66.8 ± 5.7
Gender male, n (%)	6 (75%)
BMI, kg/m^2 (mean ± SD)	28.5 ± 5.2
Smoking, n (%)	
Active	2 (25%)
Former	3 (37.5%)
Diabetes mellitus, n (%)	2 (25%)
Hypertension, n (%)	6 (75%)
History of CVD, n (%)	
Coronary heart disease	4 (50%)
Ischemic cerebral event	3 (37.5%)
Peripheral artery disease	4 (50%)
Medication, n (%)	
Statin	8 (100%)
Antihypertensive	8 (100%)
Antiplatelet	8 (100%)
Serum lipid profile	
TC, mg/dL (mean ± SD)	190.0 ± 57.1
HDL-C, mg/dL (mean ± SD)	42.0 ± 12.6
LDL-C, mg/dL (mean ± SD)	86.4 ± 17.0
Triglycerides, mg/dL (median [IQR])	103.2 [91.2–182.2]
ApoA-I, mg/dL (mean ± SD)	157.9 ± 36.7
Serum biochemistry	
Creatinine, μmol/L (mean ± SD)	80.9 ± 13.9
eGFR, mL/min/1.73 m^2 (mean ± SD)	>60 ± 0.0
Glucose, mmol/L (mean ± SD)	6.0 ± 1.2
ASAT, U/L (mean ± SD)	29.3 ± 14.6
ALAT, U/L (mean ± SD)	30.2 ± 19.7

Categorical variables are presented as numbers (%). Continuous values are expressed as mean ± standard deviation or median [interquartile range].
ApoA-I, apolipoprotein A-I; ALAT, alanine aminotransferase; ASAT, aspartate aminotransferase; BMI, body mass index; CVD, cardiovascular disease; eGFR, estimated glomerular filtration rate; HDL-C, high-density lipoprotein cholesterol; IQR, interquartile range; LDL-C, low-density lipoprotein cholesterol; TC, total cholesterol.

Next, arterial wall dimensions for each carotid artery, and for plaque and non-plaque regions was determined using CE-MRI (Fig. 4B; Data Supplement Fig. 2): 16 carotid arteries were scanned, of which 14 were of sufficient quality for analysis. One patient had a total occlusion of the common carotid artery on one side, resulting in 13 analysable carotid artery segments. As presented in Table 2, arterial wall dimensions of the carotids were thickened in our patients and comparable with previously reported values for CVD patients [29]. In addition, we identified 18 plaques in total: 13

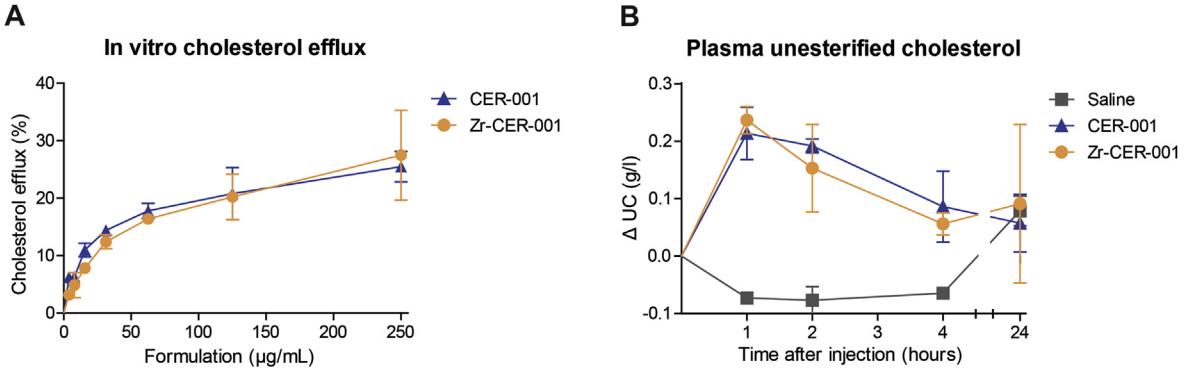

Fig. 2. Functionality of ^{89}Zr-labeled CER-001. The cholesterol mobilizing capacity of ^{89}Zr-labeled CER-001 and unlabeled CER-001 were compared. (A) *In vitro* cholesterol efflux from J774 macrophages induced by ^{89}Zr-labeled CER-001 and unlabeled CER-001. (B) Plasma unesterified cholesterol mobilization in C57Bl6/J mice after infusion of (^{89}Zr-labeled) CER-001 (n = 5 per group; n = 2 in the placebo group). UC, unesterified cholesterol.

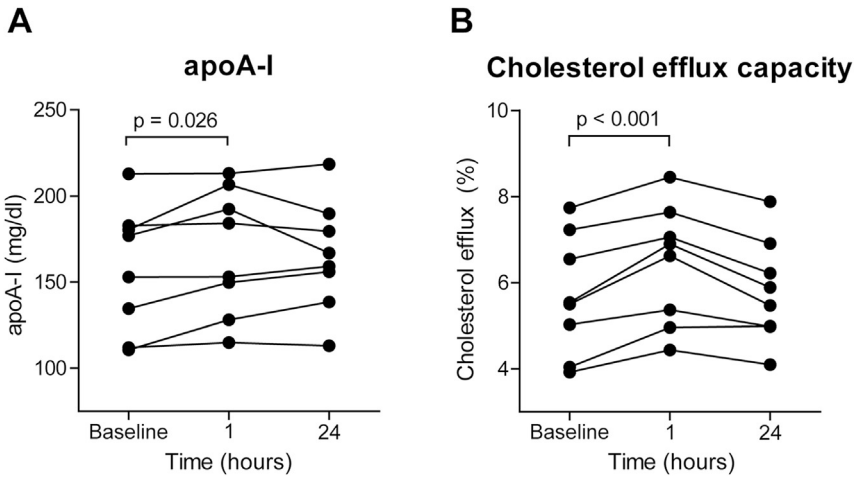

Fig. 3. ApoA-I and cholesterol efflux capacity in patients. Plasma apoA-I levels and plasma-mediated cholesterol efflux were determined at baseline, 1 and 24 h after infusion of CER-001 and ^{89}Zr-labeled CER-001 (n = 8).

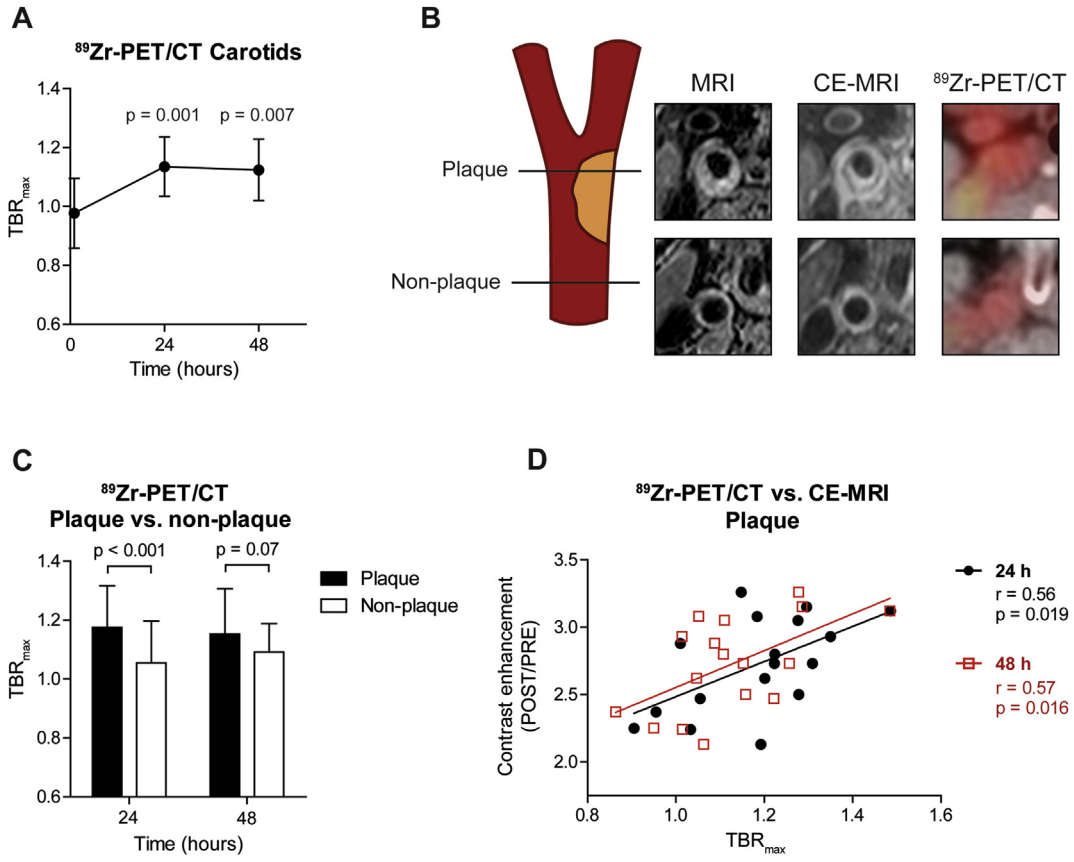

Fig. 4. Multimodality imaging of patients. (A) Graph showing changes of TBR_{max} of the carotid arteries over time as assessed with PET/CT (n = 16 for each timepoint). (B) Schematic diagram of plaque versus non-plaque analysis with corresponding representative CE-MRI and PET/CT images. (C) TBR_{max} of plaque versus non-plaque segments in the carotid arteries after 24 h (n = 18 for both plaque and non-plaque). (D) Scatterplot depicting the relationship between ^{89}Zr-labeled CER-001 PET/CT signal and delayed contrast-enhancement ratio (POST/PRE) on MRI (n = 18). TBR_{max}, target-to-background ratio.

common carotid plaques in 8 patients, and 5 internal carotid plaques in 5 patients. These plaques were clearly distinct from non-plaque regions (mean wall area 35.43 ± 10.60 and 21.39 ± 4.37, respectively; $p < 0.001$). The TBR_{max} value in plaques was significantly higher compared with the value in non-plaque areas 24 h after infusion (1.18 ± 0.14 *vs.* 1.05 ± 0.14; $p < 0.001$), with a similar trend 48 h after infusion (Fig. 4C).

In addition to plaque dimensions, CE-MRI was performed to gain insight into the contrast enhancement of the plaques: out of 18 plaques, 17 were of sufficient quality for analysis. The plaque uptake of CER-001 after 24 and 48 h as measured by PET/CT correlated with the delayed enhancement ratio (POST/PRE) on CE-MRI (24 h: r = 0.56, $p = 0.019$; 48 h: r = 0.57, $p = 0.016$; Fig. 4D).

Table 2
Arterial wall and plaque dimensions.

Arterial wall and plaque dimensions on MRI				
	Segment (number analyzed)			
	Common carotid (n = 13)	Plaque (n = 18)	Non-plaque (n = 18)	Plaque *vs.* non-plaque
Mean wall area (mm^2)	28.49 ± 5.85	35.43 ± 10.60	21.39 ± 4.37	$p < 0.001$
Mean wall thickness (mm)	1.15 ± 0.18	1.46 ± 0.40	0.98 ± 0.16	$p < 0.001$
Maximal wall thickness (mm)	3.00 ± 1.26	3.22 ± 1.34	1.58 ± 0.32	$p < 0.001$

p-values are for differences between plaque and non-plaque segments.
MRI, ma4gnetic resonance imaging.

3.6. Safety results

Infusion of ^{89}Zr-labeled CER-001 was well tolerated during the study and did not induce changes in blood pressure or heart rate. No adverse events were reported.

4. Discussion

In the present study, vessel wall imaging studies support the concept that infused HDL mimetic particles localize to advanced atherosclerotic plaques in patients. More specifically, the PET signal elicited by ^{89}Zr-labeled CER-001 was higher at sites of atherosclerotic plaques compared with sites without plaque, within the same patient. The extent of ^{89}Zr-labeled CER-001 signal in the plaque also correlated with the contrast enhancement of the plaque as measured by MRI. Together, these data suggest that determinants of plaque contrast enhancement may predict the extent of access of apoA-I HDL mimetic particles into the plaque area. Furthermore, we have shown that CER-001 enhances plasma cholesterol efflux capacity in patients, and that the chelator conjugation and ^{89}Zr-labeling of CER-001 did not influence its cholesterol efflux capacity either *in vitro* or *in vivo*.

4.1. Cardiovascular imaging with ^{89}Zr-labeled CER-001

In the field of oncology, the need to quantify targeted delivery of infused drugs has long been recognized, as the therapeutic response directly relates to the local drug concentrations achieved in tumours [30]. In patients with CVD, most therapeutic strategies have focused on systemic risk factors, thereby precluding the necessity to assess uptake of drugs in atherosclerotic lesions. However, for apoA-I-containing HDL mimetics, targeted delivery into the atherosclerotic plaque is considered to be a prerequisite to achieve therapeutic response, since the atheroprotective effect is driven by removal of cholesterol from lesional, lipid-laden macrophages [9]. To study localization of CER-001 to plaques, we used a Good Manufacturing Practice approved method of ^{89}Zr-labeling to allow for non-invasive *in vivo* imaging [31]. We demonstrated the feasibility of applying ^{89}Zr-PET to assess targeted delivery of HDL mimetics to atherosclerotic lesions in patients, as ^{89}Zr-labeling of CER-001 was safe, stable, and did not alter cholesterol mobilizing functionality. After infusion in patients with atherosclerosis, we found increased PET signal of ^{89}Zr-labeled CER-001 in atherosclerotic lesions, implying that infused unlabeled HDL mimetic particles access the intended target.

Although the passage of apoA-I through the endothelial barrier has been documented previously in humans [32], these studies were not able to differentiate between permeation of atherosclerotic lesions versus healthy arterial walls. In the present study, imaging studies point towards delivery of the apoA-I-containing HDL mimetic CER-001 in the arterial wall of patients with atherosclerotic disease. In fact, by combining MRI and PET/CT, TBR_{max} in plaques was found to be significantly higher than in non-plaque areas, implying that CER-001 particles more readily access the arterial wall at sites of atherosclerotic plaques. Moreover, the correlation between the ^{89}Zr-labeled CER-001 signal on PET and the delayed contrast enhancement signal on MRI also suggests that plaque contrast enhancement, as a surrogate marker relating to permeability, may be a determinant of delivery efficiency in atherosclerotic lesions [33]. These data concur with previous findings for permeation of liposomes across an endothelial monolayer, revealing liposomal extravasation predominantly at sites of increased endothelial permeability [34]. Collectively, our findings support the concept that apoA-I-containing HDL mimetics target atherosclerotic plaques in patients, a prerequisite for the concept of using HDL mimetic particles to enhance cholesterol efflux from lipid-laden macrophages in plaques.

Compared with results from ^{18}F-fluorodeoxyglucose (FDG) PET studies to evaluate inflammatory activity in atherosclerotic lesions, we observed only a modest increase in the carotid and plaque ^{89}Zr-signal, expressed as $TBR_{max,}$ after 24 and 48 h. This reflects the distinct behaviour of ^{18}F-FDG compared with ^{89}Zr-labeled CER-001. Whereas the glucose analogue FDG is metabolically trapped after cellular uptake in macrophages, the kinetics of apoA-I are much more complex as it has been shown to recirculate via lymph after passing the endothelial barrier [32] and has a longer blood half-life [35]. Consequently, infused ^{89}Zr-labeled CER-001 particles do not accumulate, but instead reach a steady-state level in the plaque that is determined by the in-versus outflow of the apoA-I-containing HDL mimetics. The observed differences in ^{89}Zr-signal between plaque and non-plaque regions further support these findings. Furthermore, the ^{89}Zr-labeled CER-001 signal may have been adversely affected by competition with the infused unlabeled CER-001. Indeed, such interference has been described in ^{89}Zr-antibody-based tumor imaging studies, in which target saturation may occur when the dose of the co-infused unlabeled monoclonal antibodies is too high [31]. However, considering that the amount of infused apoA-I containing CER-001 is less than 10% of endogenous plasma apoA-I, it is less likely that plaque saturation by unlabeled CER-001 contributes to the modest CER-001 signal in plaques.

4.2. HDL particles as drug carrier

Considering the key role of macrophages in the development and destabilization of atherosclerotic lesions, using nanomedicine to target macrophages is increasingly being acknowledged as an attractive approach for an effective anti-atherosclerotic therapeutic modality [36]. It has been previously shown that reconstituted HDL particles can be used as a nano-sized carrier for drug delivery into lesions, as they are very effective at delivering their payload into plaque macrophages [37,38]. Infusion of reconstituted HDL (nano) particles loaded with statins was found to exert a potent anti-atherosclerotic effect in mice, which clearly exceeded the effect attainable with oral dosing of statins [37]. Our finding of the HDL

mimetic CER-001 localizing to plaques in patients is the first clinical study finding to support the promising concept of using HDL as a nano-delivery vehicle loaded with anti-atherogenic compounds in atherosclerosis [39].

4.3. Limitations

The present study has several limitations. First, this is a single-center observational study with a small sample size. Second, we did not include a control arm of healthy volunteers in view of the radiation exposure (18 mSv). Instead, we compared plaque versus non-plaque areas within each patient, allowing us to evaluate delivery efficiency in affected versus unaffected arterial segments. Third, since high temporal resolution dynamic contrast-enhanced imaging of the carotid artery remains technologically challenging, we chose delayed enhancement imaging as a read-out of plaque permeability. Therefore, we currently cannot assess the relative contribution of different mechanisms leading to accumulation of contrast in the atherosclerotic plaque, i.e. increased endothelial permeability, plaque neovascularization, and increased extracellular space. Nevertheless, all these mechanisms will contribute to the vessel wall build-up of CER-001 and therefore do not preclude the relevance of our findings.

5. Conclusions

Here, we provide evidence to show that the HDL mimetic CER-001 enhances plasma cholesterol efflux capacity and accesses advanced atherosclerotic plaques in patients after infusion. Using non-invasive *in vivo* imaging, we observe that plaque contrast enhancement is correlated to ^{89}Zr-labeled CER-001 signal in the plaque. These data provide valuable insights for HDL mimetic infusion therapy, and may also help guide future plaque targeted delivery strategies using HDL as a nano-carrier for both imaging and therapeutic purposes in patients.

Conflict of interest

This is an investigator-initiated study, for which Cerenis provided (unlabeled) CER-001 and performed functionality testing free of charge. JL.D., R.B., R.B., and C.K. are employed by Cerenis. E.S. has received lecturing fees from Amgen, Sanofi and Merck. E.S. also served as principal investigator for the MODE and SAMBA studies (involving CER-001). All other authors besides Cerenis employees declare that they have no conflict of interest and no relationships with industry relevant to this study.

Financial support

This work was supported by a European Framework Program 7 grant (E.S: FP7-Health 309820: Nano-Athero).

Acknowledgements

The authors thank J.H.M. Levels for his work on plasma lipid analysis and stability testing, and T.C. de Wit for technical assistance.

Appendix A. Supplementary data

Supplementary data related to this article can be found at http://dx.doi.org/10.1016/j.atherosclerosis.2016.05.038.

References

[1] E. Di Angelantonio, N. Sarwar, P. Perry, S. Kaptoge, K.K. Ray, A. Thompson, A.M. Wood, S. Lewington, N. Sattar, C.J. Packard, R. Collins, S.G. Thompson, J. Danesh, Major lipids, apolipoproteins, and risk of vascular disease, JAMA 302 (2009) 1993–2000.
[2] J.C. van Capelleveen, H.B. Brewer, J.J.P. Kastelein, G.K. Hovingh, Novel therapies focused on the high-density lipoprotein particle, Circ. Res. 114 (2014) 193–204.
[3] W.E. Boden, J.L. Probstfield, T. Anderson, B.R. Chaitman, P. Desvignes-Nickens, K. Koprowicz, R. McBride, K. Teo, W. Weintraub, Niacin in patients with low HDL cholesterol levels receiving intensive statin therapy, N. Engl. J. Med. 365 (2011) 2255–2267.
[4] M.J. Landray, R. Haynes, J.C. Hopewell, S. Parish, T. Aung, J. Tomson, K. Wallendszus, M. Craig, L. Jiang, R. Collins, J. Armitage, Effects of extended-release niacin with laropiprant in high-risk patients, N. Engl. J. Med. 371 (2014) 203–212.
[5] P.J. Barter, M. Caulfield, M. Eriksson, S.M. Grundy, J.J.P. Kastelein, M. Komajda, J. Lopez-Sendon, L. Mosca, J.-C. Tardif, D.D. Waters, C.L. Shear, J.H. Revkin, K.A. Buhr, M.R. Fisher, A.R. Tall, B. Brewer, Effects of torcetrapib in patients at high risk for coronary events, N. Engl. J. Med. 357 (2007) 2109–2122.
[6] G.G. Schwartz, A.G. Olsson, M. Abt, C.M. Ballantyne, P.J. Barter, J. Brumm, B.R. Chaitman, I.M. Holme, D. Kallend, L.A. Leiter, E. Leitersdorf, J.J.V. McMurray, H. Mundl, S.J. Nicholls, P.K. Shah, J.-C. Tardif, R.S. Wright, Effects of dalcetrapib in patients with a recent acute coronary syndrome, N. Engl. J. Med. 367 (2012) 2089–2099.
[7] G.K. Hovingh, D.J. Rader, R.A. Hegele, HDL re-examined, Curr. Opin. Lipidol. 26 (2015) 127–132.
[8] A.G. Holleboom, L. Jakulj, R. Franssen, J. Decaris, M. Vergeer, J. Koetsveld, J. Luchoomun, A. Glass, M.K. Hellerstein, J.J.P. Kastelein, G.K. Hovingh, J.A. Kuivenhoven, A.K. Groen, S.M. Turner, E.S.G. Stroes, In vivo tissue cholesterol efflux is reduced in carriers of a mutation in APOA1, J. Lipid Res. 54 (2013) 1964–1971.
[9] R.S. Rosenson, H.B. Brewer, W.S. Davidson, Z.A. Fayad, V. Fuster, J. Goldstein, M. Hellerstein, X.-C. Jiang, M.C. Phillips, D.J. Rader, A.T. Remaley, G.H. Rothblat, A.R. Tall, L. Yvan-Charvet, Cholesterol efflux and atheroprotection: advancing the concept of reverse cholesterol transport, Circulation 125 (2012) 1905–1919.
[10] A. Rohatgi, A. Khera, J.D. Berry, E.G. Givens, C.R. Ayers, K.E. Wedin, I.J. Neeland, I.S. Yuhanna, D.R. Rader, J.A. de Lemos, P.W. Shaul, HDL cholesterol efflux capacity and incident cardiovascular events, N. Engl. J. Med. 371 (2014), 141118051511004.
[11] R.K. Tangirala, K. Tsukamoto, S.H. Chun, D. Usher, E. Puré, D.J. Rader, Regression of atherosclerosis induced by liver-directed gene transfer of apolipoprotein A-I in mice, Circulation 100 (1999) 1816–1822.
[12] J.J. Badimon, L. Badimon, V. Fuster, Regression of atherosclerotic lesions by high density lipoprotein plasma fraction in the cholesterol-fed rabbit, J. Clin. Investig. 85 (1990) 1234–1241.
[13] Y. Zhang, I. Zanotti, M.P. Reilly, J.M. Glick, G.H. Rothblat, D.J. Rader, Overexpression of apolipoprotein A-I promotes reverse transport of cholesterol from macrophages to feces in vivo, Circulation 108 (2003) 661–663.
[14] R.M. Stoekenbroek, E.S. Stroes, G.K. Hovingh, ApoA-I mimetics, Handb. Exp. Pharmacol. 224 (2015) 631–648.
[15] J.A. Shaw, A. Bobik, A. Murphy, P. Kanellakis, P. Blombery, N. Mukhamedova, K. Woollard, S. Lyon, D. Sviridov, A.M. Dart, Infusion of reconstituted high-density lipoprotein leads to acute changes in human atherosclerotic plaque, Circ. Res. 103 (2008) 1084–1091.
[16] S.E. Nissen, T. Tsunoda, E.M. Tuzcu, P. Schoenhagen, C.J. Cooper, M. Yasin, G.M. Eaton, M.A. Lauer, W.S. Sheldon, C.L. Grines, S. Halpern, T. Crowe, J.C. Blankenship, R. Kerensky, Effect of recombinant ApoA-I Milano on coronary atherosclerosis in patients with acute coronary syndromes: a randomized controlled trial, JAMA 290 (2003) 2292–2300.
[17] J.-C. Tardif, J. Grégoire, P.L. L'Allier, R. Ibrahim, J. Lespérance, T.M. Heinonen, S. Kouz, C. Berry, R. Basser, M.-A. Lavoie, M.-C. Guertin, J. Rodés-Cabau, Effects of reconstituted high-density lipoprotein infusions on coronary atherosclerosis: a randomized controlled trial, JAMA 297 (2007) 1675–1682.
[18] J.-C. Tardif, C.M. Ballantyne, P. Barter, J.-L. Dasseux, Z.A. Fayad, M.-C. Guertin, J.J.P. Kastelein, C. Keyserling, H. Klepp, W. Koenig, P.L. L'Allier, J. Lespérance, T.F. Lüscher, J.F. Paolini, A. Tawakol, D.D. Waters, Effects of the high-density lipoprotein mimetic agent CER-001 on coronary atherosclerosis in patients with acute coronary syndromes: a randomized trial†, Eur. Heart J. 35 (2014) 3277–3286.
[19] Y. Kataoka, J. Andrews, M. Duong, T. Nguyen, N. Schwarz, J. Fendler, R. Puri, J. Butters, C. Keyserling, J.F. Paolini, J.-L. Dasseux, S.J. Nicholls, Abstract 12156: greater regression of coronary atherosclerosis with the pre-beta high-density lipoprotein mimetic CER-001 in patients with more extensive plaque burden, Circulation 132 (2015) A12156.
[20] R.S. Kootte, L.P. Smits, F.M. van der Valk, J.-L. Dasseux, C.H. Keyserling, R. Barbaras, J.F. Paolini, R.D. Santos, T.H. van Dijk, G.M. Dallinga, A.J. Nederveen, W.J.M. Mulder, G.K. Hovingh, J.J.P. Kastelein, A.K. Groen, E.S. Stroes, Effect of open-label infusion of an apoA-I-containing particle (CER-001) on RCT and artery wall thickness in patients with FHA, J. Lipid Res. 56 (2015) 703–712.
[21] G.K. Hovingh, L.P. Smits, C. Stefanutti, H. Soran, S. Kwok, J. de Graaf, D. Gaudet,

C.H. Keyserling, H. Klepp, J. Frick, J.F. Paolini, J.-L. Dasseux, J.J.P. Kastelein, E.S. Stroes, The effect of an apolipoprotein A-I-containing high-density lipoprotein-mimetic particle (CER-001) on carotid artery wall thickness in patients with homozygous familial hypercholesterolemia: the modifying orphan disease evaluation (MODE) study, Am. Heart J. 169 (2015) 736–742 e1.

[22] Y. Huang, J.A. DiDonato, B.S. Levison, D. Schmitt, L. Li, Y. Wu, J. Buffa, T. Kim, G.S. Gerstenecker, X. Gu, C.S. Kadiyala, Z. Wang, M.K. Culley, J.E. Hazen, A.J. Didonato, X. Fu, S.Z. Berisha, D. Peng, T.T. Nguyen, S. Liang, C.-C. Chuang, L. Cho, E.F. Plow, P.L. Fox, V. Gogonea, W.H.W. Tang, J.S. Parks, E.A. Fisher, J.D. Smith, S.L. Hazen, An abundant dysfunctional apolipoprotein A1 in human atheroma, Nat. Med. 20 (2014) 193–203.

[23] B. Shao, C. Tang, A. Sinha, P.S. Mayer, G.D. Davenport, N. Brot, M.N. Oda, X.-Q. Zhao, J.W. Heinecke, Humans with atherosclerosis have impaired ABCA1 cholesterol efflux and enhanced high-density lipoprotein oxidation by myeloperoxidase, Circ. Res. 114 (2014) 1733–1742.

[24] A. Shaish, G. Keren, P. Chouraqui, H. Levkovitz, D. Harats, Imaging of aortic atherosclerotic lesions by (125)I-LDL, (125)I-oxidized-LDL, (125)I-HDL and (125)I-BSA, Pathobiology 69 (2001) 225–229.

[25] J.C. Frias, K.J. Williams, E.A. Fisher, Z.A. Fayad, Recombinant HDL-like nanoparticles: a specific contrast agent for MRI of atherosclerotic plaques, J. Am. Chem. Soc. 126 (2004) 16316–16317.

[26] M.J.W.D. Vosjan, L.R. Perk, G.W.M. Visser, M. Budde, P. Jurek, G.E. Kiefer, G.A.M.S. van Dongen, Conjugation and radiolabeling of monoclonal antibodies with zirconium-89 for PET imaging using the bifunctional chelate p-isothiocyanatobenzyl-desferrioxamine, Nat. Protoc. 5 (2010) 739–743.

[27] J.H.F. Rudd, K.S. Myers, S. Bansilal, J. Machac, C.A. Pinto, C. Tong, A. Rafique, R. Hargeaves, M. Farkouh, V. Fuster, Z.A. Fayad, Atherosclerosis inflammation imaging with 18F-FDG PET: carotid, iliac, and femoral uptake reproducibility, quantification methods, and recommendations, J. Nucl. Med. 49 (2008) 871–878.

[28] M. de la Llera-Moya, D. Drazul-Schrader, B.F. Asztalos, M. Cuchel, D.J. Rader, G.H. Rothblat, The ability to promote efflux via ABCA1 determines the capacity of serum specimens with similar high-density lipoprotein cholesterol to remove cholesterol from macrophages, Arterioscler. Thromb. Vasc. Biol. 30 (2010) 796–801.

[29] R. Duivenvoorden, E. de Groot, B.M. Elsen, J.S. Laméris, R.J. van der Geest, E.S. Stroes, J.J.P. Kastelein, A.J. Nederveen, In vivo quantification of carotid artery wall dimensions: 3.0-Tesla MRI versus B-mode ultrasound imaging, Circ. Cardiovasc. Imaging 2 (2009) 235–242.

[30] G.A.M.S. van Dongen, M.J.W.D. Vosjan, Immuno-positron emission tomography: shedding light on clinical antibody therapy, Cancer Biother. Radiopharm. 25 (2010) 375–385.

[31] G.A. Van Dongen, M.C. Huisman, R. Boellaard, N. Harry Hendrikse, A.D. Windhorst, G.W. Visser, C.F. Molthoff, D.J. Vugts, 89Zr-immuno-PET for imaging of long circulating drugs and disease targets: why, how and when to be applied? Q. J. Nucl. Med. Mol. Imaging Off. Publ. Ital. Assoc. Nucl. Med. [and] Int. Assoc. Radiopharmacol. (IAR), [and] Sect. Soc. Radiopharm. 59 (2015) 18–38.

[32] M.N. Nanjee, C.J. Cooke, R. Garvin, F. Semeria, G. Lewis, W.L. Olszewski, N.E. Miller, Intravenous apoA-I/lecithin discs increase pre-beta-HDL concentration in tissue fluid and stimulate reverse cholesterol transport in humans, J. Lipid Res. 42 (2001) 1586–1593.

[33] C. Calcagno, S. Ramachandran, A. Millon, P.M. Robson, V. Mani, Z. Fayad, Gadolinium-based contrast agents for vessel wall magnetic resonance imaging (MRI) of atherosclerosis, Curr. Cardiovasc. Imaging Rep. 6 (2013) 11–24.

[34] Y. Kim, M.E. Lobatto, T. Kawahara, B. Lee Chung, A.J. Mieszawska, B.L. Sanchez-Gaytan, F. Fay, M.L. Senders, C. Calcagno, J. Becraft, M. Tun Saung, R.E. Gordon, E.S.G. Stroes, M. Ma, O.C. Farokhzad, Z.A. Fayad, W.J.M. Mulder, R. Langer, Probing nanoparticle translocation across the permeable endothelium in experimental atherosclerosis, Proc. Natl. Acad. Sci. U. S. A. 111 (2014) 1078–1083.

[35] E.J. Schaefer, L.A. Zech, L.L. Jenkins, T.J. Bronzert, E.A. Rubalcaba, F.T. Lindgren, R.L. Aamodt, H.B. Brewer, Human apolipoprotein A-I and A-II metabolism, J. Lipid Res. 23 (1982) 850–862.

[36] M.E. Lobatto, V. Fuster, Z.A. Fayad, W.J.M. Mulder, Perspectives and opportunities for nanomedicine in the management of atherosclerosis, Nat. Rev. Drug Discov. 10 (2011) 835–852.

[37] R. Duivenvoorden, J. Tang, D.P. Cormode, A.J. Mieszawska, D. Izquierdo-Garcia, C. Ozcan, M.J. Otten, N. Zaidi, M.E. Lobatto, S.M. van Rijs, B. Priem, E.L. Kuan, C. Martel, B. Hewing, H. Sager, M. Nahrendorf, G.J. Randolph, E.S.G. Stroes, V. Fuster, E.A. Fisher, Z.A. Fayad, W.J.M. Mulder, A statin-loaded reconstituted high-density lipoprotein nanoparticle inhibits atherosclerotic plaque inflammation, Nat. Commun. 5 (2014) 3065.

[38] J. Tang, M.E. Lobatto, L. Hassing, S. van der Staay, S.M. van Rijs, C. Calcagno, M.S. Braza, S. Baxter, F. Fay, B.L. Sanchez-Gaytan, R. Duivenvoorden, H.B. Sager, Y.M. Astudillo, W. Leong, S. Ramachandran, G. Storm, C. Perez-Medina, T. Reiner, D.P. Cormode, G.J. Strijkers, E.S.G. Stroes, F.K. Swirski, M. Nahrendorf, E.A. Fisher, Z.A. Fayad, W.J.M. Mulder, Inhibiting macrophage proliferation suppresses atherosclerotic plaque inflammation, Sci. Adv. 1 (2015) e1400223–e1400223.

[39] M.A. Lameijer, J. Tang, M. Nahrendorf, R.H.J. Beelen, W.J.M. Mulder, Monocytes and macrophages as nanomedicinal targets for improved diagnosis and treatment of disease, Expert Rev. Mol. Diagn. 13 (2013) 567–580.